

Effect of Low-Temperature Plasma Treatment on Starch-Based Biochar and Its Reinforcement for Three-Dimensional Printed Polypropylene Biocomposites

Zaheeruddin Mohammed, Shaik Jeelani, and Vijaya K. Rangari*

Cite This: *ACS Omega* 2022, 7, 39636–39647

Read Online

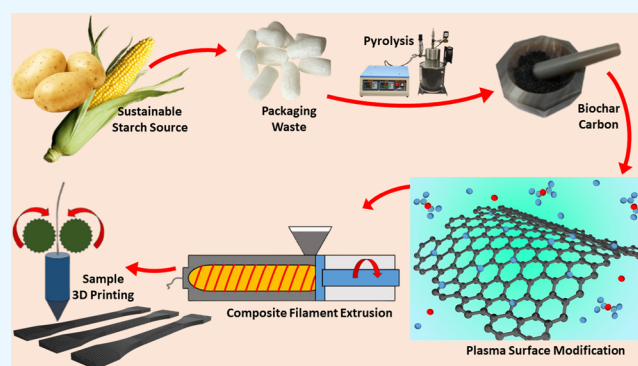
ACCESS |

Metrics & More

Article Recommendations

Supporting Information

ABSTRACT: Uniform dispersion and high interfacial adhesion are two of the most difficult components of creating an ideally reinforced polymer composite. One of the solutions could be surface engineering of reinforcing filler materials utilizing innovative technologies. Low-temperature plasma treatments in the presence of sulfur hexafluoride (SF₆) gas are proposed as a sustainable alternative to modify the surface properties of biochar carbon synthesized from sustainable starch-based packaging waste via a high-temperature/pressure pyrolysis reaction in the current study. X-ray photoelectron spectroscopy tests revealed that plasma treatments were effective in the fluorination of biochar carbon like wet chemical methods. By delivering fluorine-related functionalities only on the surface of the carbon, plasma treatments were efficient in changing the surface properties of biochar carbon while keeping the carbon's beneficial bulk properties intact, which is unique to this method. The modified biochar was effectively utilized to reinforce polypropylene. Mechanical properties like tensile strength improved by 91% when compared to neat polymers and 31% when compared to untreated biochar-reinforced polymers at 0.75 wt % loadings. Elongation at break increased from 12.7 to 38.78, showing an impressive 216% increase due to effective reinforcement by plasma functionalization. The decomposition onset temperature and maximum rate of decomposition temperature increased by 60 and 49 °C, respectively, when compared to neat polymers. Plasma-modified biochar-reinforced three-dimensional printed samples have shown promise to be utilized for the development of composite parts using additive manufacturing methods.



INTRODUCTION

The sharp increase in problems associated with global warming, environmental pollution, and depleting fossil fuel resources has created the need for the development of material systems and fabrication processes that are sustainable.^{1–3} Plant- and animal-based materials are being rapidly explored as alternative materials for various applications.^{4–8} Reinforcing polymer matrices with inexpensive sustainable carbon filler materials has been explored rigorously in the past by researchers particularly to mitigate dependency on fossil fuel-based reinforcing fillers like carbon nanotubes and graphene nanoplatelets.^{9–12} The reinforcing ability of biochar carbon mainly depends on the inherent strength of the fillers and mechanical interlocking between the filler and host polymer matrix. For this reason, biochar with microsize pores is preferred to create effective interlocking.^{13,14} However, such biochars with micropores due to their relatively poor mechanical, thermal, and electrical properties are loaded in huge weight percentages (15–30%) to create a composite with improved properties.

Poulose et al. used date palm waste-derived biochar to reinforce polypropylene (PP) at a loading of up to 15%. It was found that biochar was effective in improving the electrical conductivity and tensile modulus of the system.¹⁵ In another study, Zhang et al. used a softwood-based material to derive poplar biochar at different temperatures to reinforce polyethylene (PE). They have loaded PE with a biochar loading of up to 70 wt %. It was revealed that the interlocking effect between the filler and matrix was the primary reason for mechanical property enhancement.¹⁶ Similar studies were performed by Bhattacharyya and co-workers where they have used multiple biochars to reinforce PP. A general improvement in mechanical and thermal properties was reported.^{17,18} Engineered biochar carbon with improved structural and

Received: April 15, 2022

Accepted: July 26, 2022

Published: October 24, 2022



chemical morphology to improve the overall mechanical and thermal properties of the composite can be developed. Rice husk-derived biochar was activated with H_3PO_4 at different concentrations, and the effect it had on the morphology of carbon was investigated. It was revealed that biochar with the highest porous morphology was the most effective in its reinforcing ability, thus improving the overall thermal and mechanical properties of the system.¹⁹ High-pressure/temperature pyrolysis reactions can be utilized to synthesize carbon with better inherent properties, thus allowing for lower loading wt %.²⁰ Idrees et al reinforced recycled poly(ethylene terephthalate) with packaging waste-derived biochar at loading as low as 0–5 wt %.²¹ The biochar can be further reduced in its size to make effective use of surface through postprocessing methods like activation,^{22,23} ultrasonication,^{24,25} and ball milling.^{26,27} However, the carbon thus produced will be limited in use particularly for reinforcement applications due to hydrophobic and inert surfaces.

In composites, generally, the major challenge while reinforcing with micro/nanosize reinforcements is that the fillers tend to agglomerate due to van der Waals forces and lack of proper interface between the filler and matrix. This limits the load/heat transfer at the filler/matrix interface.^{28–30} Thus, the ability of the filler to effectively reinforce largely depends on the compatibility of the filler and matrix in the material system.^{31–33} Introducing surface functional groups on the surface of the filler material is often considered as a viable solution to address these issues. It not only reduces the degree of agglomerations by enhancing dispersibility but also ensures a better interface between the reinforcing filler and host matrix. The density, distribution, and type of functional group introduced on the surface of filler surfaces will provide synergistic effects to control interfaces across the composite material systems.^{34–38} Several methods of surface functionalization have been implemented, which mainly consist of wet chemistry methods. These methods are relatively expensive and, in many cases, not very environmentally friendly. There are many approaches to fine-tune the surface properties like covalent, noncovalent, and defect functionalization. However, these approaches tend to deteriorate the desirable properties of carbon sometimes.^{39–42}

To overcome these problems, researchers are exploring new methods to improve the surface properties of carbon materials without affecting their bulk properties. Because it creates chemically active species on the surface, the plasma process is seen as a promising method for altering the chemical surface characteristics of carbon materials.^{43,44} Electrons, ions, atoms, and molecules that are partially or completely ionized in gas form the basis of plasma.^{45–47} In terms of functionalization, plasma procedures have several advantages over traditional approaches. Plasma modification techniques drastically shorten processing times and reagent requirements, excluding functionality relevant to the surface. The method of plasma functionalization is adaptable, quick, and clean.^{48,49} The slower chemical reactions with the chemically active species happen exclusively on the surface of the carbon material during plasma operations; they do not affect the bulk properties at low atmospheres with protracted application times. By using various gas sources in plasma processes, acidic and basic functional groups can be introduced on the surface of carbon-based materials.^{50–52} Excited molecules and radicals react with surface-bound carbon double bonds during plasma interactions to provide open ends and imperfect sites for functionalization.

The features of a carbon material that functional groups introduce into its surface help in not only good interactions but also the dispersion of fillers in organic and aqueous solutions as well as polymer matrices.^{46,53} By optimizing parameters such as application power, dielectric thickness, application time, and type of gas used during plasma processing, different functional groups can be formed. The plasma treatment approach has also been explored to modify the surface properties of biochar carbon. Rice husk-derived biochar was modified using plasma treatments in the presence of different gas sources. The type of gas has a considerable impact on the kind of surface modification that can be accomplished through plasma treatments.⁵⁴ For efficient mercury removal, active C–Cl groups were implanted on the surface of biochar using low-temperature plasma with chlorine.⁵⁵ Therefore, it can be concluded that low-temperature plasma treatments are efficient, affordable, and less-laborious ways to change the surface characteristics of carbonaceous biochar.

PP is considered as one of the important utility polymers considering its wide range of applications in the field of automotive, aerospace, and everyday electrical appliances. However, PP generated via bulk polymerization often has low mechanical and thermal properties. Aside from its lack of usable qualities, PP has been reported to have difficulties being used as a three-dimensional (3D) printing material, owing to its semicrystalline form.⁵⁶ Due to its tendency to shrink and distort, fabricating PP specimens using additive manufacturing processes with acceptable dimensional stability is difficult.⁵⁷ As additive manufacturing prepares to disrupt the manufacturing business, researchers throughout the world are working to produce materials that can be printed, as well as parts that are comparable to or better than parts made using traditional methods, including with multifunctionality with the advent of four-dimensional printing.⁵⁸ There are several approaches to minimize shrinkage or warpage of 3D printed PP parts, some of them being decreasing the crystallinity of the material, blending, or making changes to print methodology. Recently, materials scientists are exploring the use of filler materials as they can act as nucleating agents influencing the crystallinity of the polymer and affecting polymer chain conformations.⁵⁹

Reinforcing PP with a carbon-based filler while having an effective interface, optimal load transfer, and thermal interactions between the constituent materials can be achieved.^{60–62} Using plasma technology to effectively fluorinate carbon material surfaces has been demonstrated in the literature. It was reported that plasma fluorinated carbons develop an efficient coating without altering the bulk properties. This effect can be more pronounced in terms of biochar kind amorphous carbons as there will be more defective sites readily available.^{63,64} Fluorinated carbons can be an ideal reinforcement material as they have the potential to better interface. The supporting principle for this was presented by Shofner et al.⁶⁵ in their studies incorporating fluorinated single-wall carbon nanotubes (F-SWNT) in PE. They proposed the reaction scheme in which the loss of a fluorine moiety during the melt processing stage acts as a catalyst for the subsequent linkage of the carbon to the surrounding polymer matrix. In another similar study, a PP polymer was reinforced with SWNT;⁶⁶ in the case of the PP/F-SWNT composite system, an enhanced chemical interaction was expected due to the presence of more reactive tertiary C–H bonds in the PP structure and a higher melt processing temperature. Biochar carbon fluorinated via a sustainable

plasma process can help carbon covalently react with the surrounding PP polymer via an in situ reaction initiated during the extrusion process.

In continuation of our earlier work,⁶⁷ where pyrolyzed biochar was modified for size reduction and surface area increase through ultrasonication, here, for the first time, we explore the possibility of sustainable plasma fluorinated biochar carbon to covalently interact with the host PP matrix forming an effective interface. In the present work, sustainable packaging waste (made from starch) derived from biochar carbon is surface modified using a sustainable plasma treatment process. The carbon thus obtained was used as a reinforcing filler for the PP matrix. The addition of biochar at very low percentage loadings unlike conventional higher biochar loadings proved to improve the mechanical and thermal properties of the biocomposite.

EXPERIMENTAL SECTION

Materials. Ecolpack (Japan) provided a peanut-shaped loose filler packaging waste (PW) material (Bran Foam Top), which was mostly comprised of starch and supplied as packaging for scientific equipment. A PP matrix with an isotactic crystalline structure, a molecular weight of 40,000–100,000, a powder diameter of $\sim 20 \mu\text{m}$, and a density of 0.910 to 0.928 g/cm^3 was obtained from Chem Point (USA).

Biochar Carbon Synthesis. Biochar was derived from starch-based PW via pyrolysis reaction using a high-temperature/pressure reactor. PW powder was pyrolyzed at a rate of $10 \text{ }^\circ\text{C}/\text{min}$ up to $1100 \text{ }^\circ\text{C}$ and then kept at that temperature for 3 h under an autogenic pressure of 150 bar. The synthesized biochar was further engineered for size reduction and improved surface area using the ultrasonication process. The detailed process of biochar synthesis and postprocessing using ultrasonic reaction are discussed in an earlier study.⁶⁷

Plasma Functionalization. PE-100 equipment from Plasma Etch was used for LTP treatments. The design of machine was custom modified with a rotating circular drum as a sample holder to ensure uniform functionalization of powdered materials. Carbon was plasma treated in the presence of sulfur hexafluoride (SF_6) gas at a chamber pressure of 0.2 mTorr and at a constant flow of 5 ccm, and an RF power of 150 W was generated at a standard frequency of 13.5 MHz for different time durations of 5, 10, 15, 20, and 30 min. A schematic diagram showing a setup of plasma treatment is shown in Figure 1.

Composite Fabrication. PP powder was dried in an oven overnight at $100 \text{ }^\circ\text{C}$ to remove any remaining moisture.

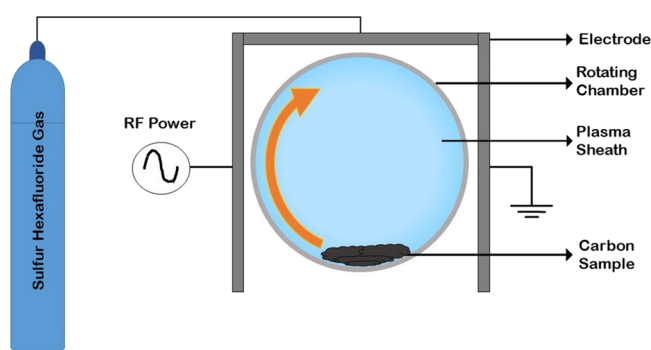


Figure 1. Schematic showing plasma treatment of PW -derived carbon in the presence of SF_6 gas.

Biochar was blended in various weight percentages ranging from 0 to 1%. Loading percentages greater than 1 wt % were not examined since higher loading percentages cause agglomeration in the composite due to increased surface area and smaller particle size. Using the manual bag approach, biochar was measured and well mixed with the PP matrix and then mechanically mixed for 5 min at 600 rpm. The combination was extruded using a single screw extruder (EX2 Filabot with screw $L/D = 12$ and pitch 12 inch) at $230 \text{ }^\circ\text{C}$ and a screw speed of 20 rpm (Figure 1 Supplementary Material). The extruded filaments were pelletized using a Filabot pelletizer. The pellets were then extruded into uniform filaments of diameter 1.7–1.75 mm under the same conditions in the same extruder to ensure homogeneous carbon biochar dispersion in PP.

3D Printing of Samples. The extruded filaments were utilized to 3D print specimens with a Hydra16A 3D printer system from Hyrel 3D (GA, USA) and an MK450 hot head, which is equipped with a high torque stepping motor to aid in material printing. The 3D models of test specimens were created with FreeCAD software and then sliced with Slic3r (Figure 2). For tensile testing, dog bone (Type 1BA)-shaped samples were printed according to ISO 527-2 (Figure 2 Supplementary Material). Objects were printed with two perimeters and a $0/90^\circ$ infill type with 100% fill. The following printing parameters were specified using the Slic3r software: nozzle diameter: 0.6 mm; layer height: 0.40 mm; nozzle temperature: $210 \text{ }^\circ\text{C}$ ($+10 \text{ }^\circ\text{C}$ for composite). The printing speed was fixed at 50 mm/s (Supplementary Video).

Materials Characterization. Biochar Carbon Characterization. A Panalytical Empyrean system with a Cu anode ($=1.54187$) was used to perform X-ray diffraction (XRD) investigation at 40 kV, 30 mA, and 1.2 kW. The incident optic was a Cu K-beta reduction incident optic with a $1/8^\circ$ divergence slit and a $1/2^\circ$ antiscatter slit. In scanning line mode, a Pixel 3D detector was employed. The diffraction data for the biochar sample were taken at a scan rate of $2^\circ/\text{min}$ in the 2θ range ($10\text{--}70^\circ$). To evaluate the graphitization degree and analyze graphitic and defective carbon, a Thermo Scientific DXR Raman spectroscopy instrument was used to get the Raman spectrum for the biochar. A laser with a 785 nm excitation wavelength is included in the system. With a laser power of 5.0 mW, the spectrum was acquired in the range of $500\text{--}2500 \text{ cm}^{-1}$.

A transmission electron microscope was used to examine the microstructure of biochar carbon (TEM-Jeol 2010). Carbon was disseminated in ethanol using an ultrasonic bath, then dispensed over a Cu grid, and dried by air. The TEM examination was carried out at a voltage of 200 kV. Using a JEOL JSM-7200F field emission scanning electron microscope, the surface morphology of biochar was examined (FESEM, JEOL USA). To generate a conductive surface, the samples were sputter-coated with gold/palladium (Au/Pd) for 3 min at 10 mA using a Hummer sputter coater. Using ImageJ software, particle sizes were calculated using the same SEM images.

Using Phi Electronics, Inc., X-ray photoelectron spectroscopy (XPS) tests were conducted on carbon to assess surface binding energies and the attachment of fluorine functionalities. Versaprobe 5000 features a monochromatic Al X-ray source with a spot size of $100 \mu\text{m}$ and a power of 25 W. Because the system includes dual charge neutralization, no adjustments to the peak positions were made. With a step size of 0.8 eV and a pass energy of 187.85 eV, survey scans were performed. With a

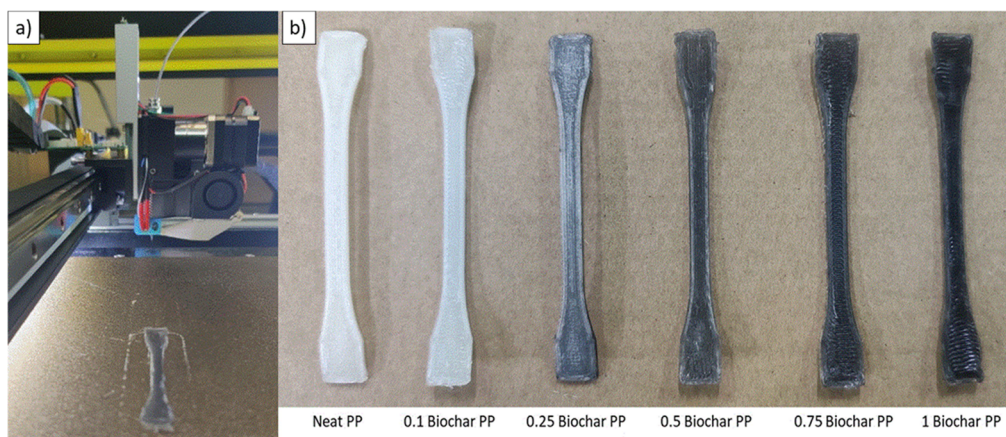


Figure 2. (a) 3D printing setup and (b) printed samples with different loading percentages.

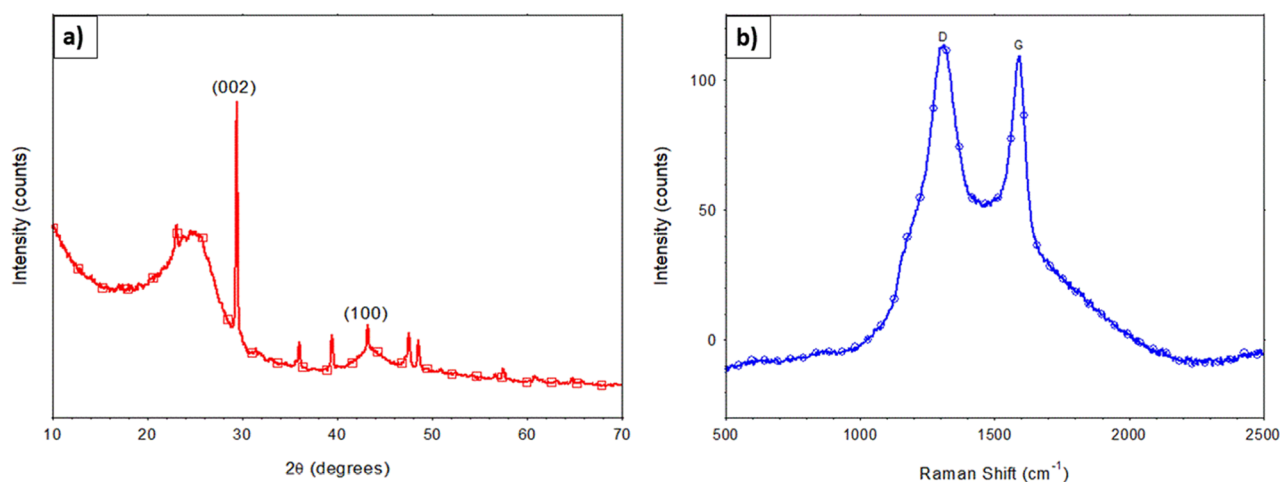


Figure 3. (a) XRD graph; (b) Raman spectra of 30 min plasma-treated biochar carbon.

0.1 eV step size and a pass energy of 23.5 eV, high-resolution scans were performed.

Composite Characterization. The mechanical properties of the filaments were determined using a Zwick/Roell Z2.5 Universal Mechanical Testing-Machine with a 2.5 kN load cell. At least five specimens of each kind were tensile tested according to the ASTM D3379 standard. The filaments were tested with a gauge length of 40 mm, 0.1 N preload tension, and a test speed of 0.5 mm/min. Similarly, a gauge length of 20 mm, a preload tension of 1 N, and a test speed of 5 mm/min were used for tensile testing of 3D printed dog bone-shaped specimens. With the help of the TestXpert data collecting and analysis software, the tensile characteristics like the modulus, tensile strength, and elongation at break were computed. To quantify strain, the crosshead displacement method was used. The effect of biochar reinforcement on the material's thermal stability and the residue was examined using TA Instruments' Q-500 thermogravimetric analysis (TGA). The apparatus was purged at a rate of 90 mL/min using dry nitrogen. Samples were scanned at a rate of 10 °C/min from 30 to 800 °C, with data on sample weight loss recorded as a function of temperature. Each test yielded sample weight loss and derivative weight loss curves, as well as thermal stability indicators such as onset and decomposition temperatures, as well as residues for each sample. Differential scanning calorimetry (DSC) was performed with a TA Instruments

Q2000 DSC machine in nonisothermal mode at 10 °C/min. Each sample was sealed in an aluminum pan with a weight of 6–8 mg, and the test was performed against an empty reference pan. To remove thermal history, they were first heated from (30 to 250 °C) at a rate of 10 °C/min and then cooled to 30 °C at the same rate. The thermal analysis was carried out in a nitrogen (N₂) environment at a flow rate of 50 cm³/min to avoid any thermal degradation of the materials. Based on the second heating and first cooling cycle, the melting temperature, crystallization temperature, and melting enthalpy were calculated using the TA-Analysis software tool. The melting enthalpy (ΔH_m) of each sample was compared to the value for 100% crystalline PP (ΔH_m°) to determine the degree of crystallinity of materials. The total enthalpy approach was used to calculate the crystallinity percentage of each sample, which was based on the equation below.

$$\chi_c(\%) = \frac{\Delta H_m}{(1 - \varphi)\Delta H_m^\circ} \times 100$$

where (χ_c) is the degree of crystallinity, (ΔH_m) is the sample melting enthalpy, (ΔH_m°) is the enthalpy of melting of 100% crystalline neat PP (207 J/g), and φ is the weight fraction of BC in the composite.⁶⁸

RESULTS AND DISCUSSION

An XRD plot of plasma-treated pyrolytic biochar carbon is shown in Figure 3a. There is a clear sharp peak near 29° corresponding to the (002) plane with an interlayer spacing of 0.30 nm, and the full width of half of the maximum value of the 100% peak is considered to be 0.0033 radians. Hence, the nature of carbon can be considered graphitic. The graphitization of carbon in this type of biochar was primarily due to the pyrolysis process. The slow pyrolysis rate promoted the aromatization of the hydrocarbon chains, and the high-temperature/high-pressure conditions and a retention time of 3 h further promoted the turbostratic arrangement of the carbon surface. This can be seen at the (100) peak of 42° . However, the presence of a broad peak near 24° indicates the presence of an amorphous (early weakly crystalline) carbon phase within the material, typical of biochar materials. The lack of a clear peak on the (101) plane near 45° indicates that the carbon obtained in this study is not entirely graphite. The present XRD pattern of plasma-treated carbon is very similar to the XRD pattern of untreated carbon,⁶³ indicating that plasma treatment did not affect the bulk properties of the carbon. Raman spectroscopy and TEM microstructure analysis were performed to further confirm the effect of plasma treatment on the bulk properties of biochar.

Raman spectroscopy results of the plasma-treated biochar shown in Figure 3b showed that plasma treatment did not affect bulk properties. The characteristic D and G bands corresponding to the disorder/defect and sp^2 hybrid graphite-like carbon, respectively, have been analyzed in detail. It was found that there were clear peaks for both G and D, and graphitic carbon and polycyclic aromatic hydrocarbons were confirmed, respectively. Peak carbons in the G and D bands were obtained near 1595 and 1310 cm^{-1} , respectively. We calculated the ID/IG ratio, which is the ratio of D-band to G-band intensities commonly used to assess the degree of disorder in carbonaceous materials. The ID/IG ratio was about 1.042. Such ratios indicate highly graphitized materials and are very difficult to achieve with pyrolytic carbon from biomass. The IG/ID ratio of untreated carbon was 1.04, indicating that plasma treatment had little effect on the surface crystallization of carbon from sp^2 to sp^3 due to defect site formations. However, this change is negligible, confirming that plasma treatment did not affect the bulk properties of biochar under these conditions.

TEM micrographs of biochar carbon before (Figure 4a) and after plasma treatment (Figure 4b) showed that the synthesized carbon was a combination of amorphous carbon and crystalline carbon. TEM images also confirm that plasma

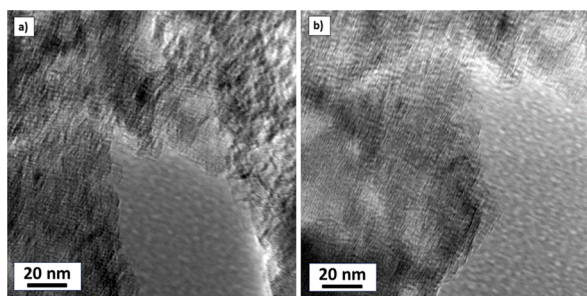


Figure 4. TEM micrographs of biochar carbon (a) untreated; (b) 30 min plasma treated.

treatment did not affect the particle size, size distribution, or morphology of the carbon surface. These TEM images are in good agreement with the XRD and Raman results. This makes it an ideal way to modify the surface properties, ensuring that plasma treatment in the presence of SF₆ does not reduce the bulk properties of the biochar, making it more suitable for forming better interfaces for composite reinforcement.

The SEM micrograph of plasma-treated carbon shown in Figure 5b revealed that there was no drastic change in the

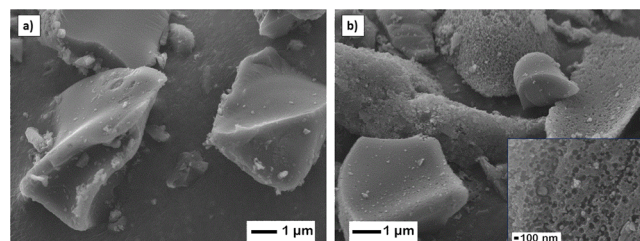


Figure 5. SEM micrographs of biochar carbon (a) untreated; (b) 30 min plasma treated.

surface morphology of the carbon when compared with the untreated carbon (Figure 5a). There was a slight surface etching of carbon, which might happen due to defect sites formed by fluorine ions when interacting with sp^2 type of graphitized carbon. Since plasma treatments are effective only on a surface level, the bulk properties of the material will not be altered.

The SF₆ plasma-treated biochar carbon for various time durations was characterized for surface binding energies using the XPS technique (Figure 6). It was found that plasma

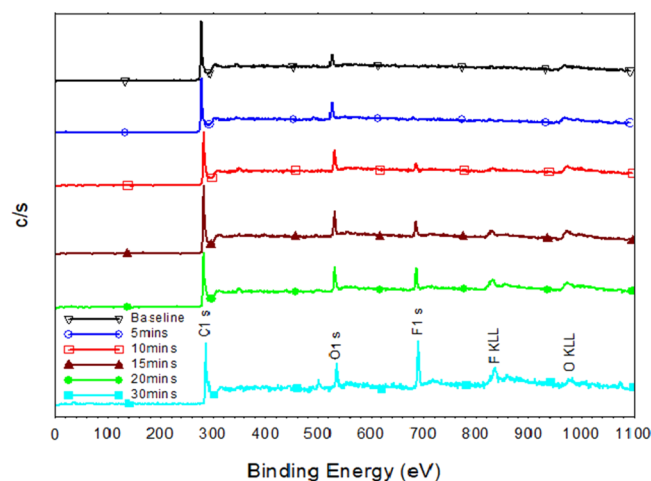


Figure 6. XPS graphs of neat and plasma-treated biochar carbon.

treatments were effective in increasing fluorine-related functional groups on the carbon surface. This enhancement can affect the hydrophilicity and reactivity of the material. The surface elemental composition of oxygen, carbon, and fluorine and O/F ratio obtained from XPS studies revealed that with an increase in treatment duration there was a decrease in carbon content and an increase in oxygen and fluorine content up to 20 min. Upon further treatments, there was a reduction in oxygen content and an increase in fluorine content. The O/F ratio, which is a good measure to look at available surface functionalities, revealed that with increased treatment time,

fluorine-related functionalities were more dominant than oxygen-related groups. The highest fluorine-related functionalities were observed in 30 min treatments as shown in Table 1. Upon further treatment, there was not any substantial

Table 1. Elemental Composition and the O/F Ratio of Carbon Fluorinated for Different Time Durations

time	C (%)	O (%)	F (%)	Na (%)	Ca (%)	S (%)	O/F
no treatment	88.1	11			0.9		
5 min	84.5	12.8	1.3	0.9	0.4	0.1	9.85
10 min	79.3	15.8	3.3		1.1	0.4	4.79
15 min	80.3	12.2	6.6	0.7		0.2	1.84
20 min	75.1	14.9	9.1		0.6	0.3	1.64
30 min	68.0	12.6	16.8	2.5			0.75

change in the functionalities of surface energy indicating saturation of the process. There were also some trace amounts of other elements, which are typical for a biochar kind of material. Thus, using the XPS technique, the quantitative presence of oxygen, carbon, and fluorine of the carbon surface was established.

The C 1s scan of the plasma-treated carbon showed peaks of the sp^2/sp^3 carbons at 284.0–285.0 eV, oxygen-grafted carbons in the form of hydroxyl and carboxyl groups at 286.71 and 288.92 eV, and a $\pi-\pi^*$ shake-up peak at 290.96 eV. The high-resolution C 1s peak scan of the 20-min plasma-treated carbon (Figure 7a) also shows carbons at 285.77 eV and oxygen-bonded carbons at 286.71 eV. Two peaks characteristic of fluorinated and oxofluorinated carbons are observed at 288.92 and 290.96 eV, respectively. For 30 min plasma treatment (Figure 7b) it can be observed that oxygen-bonded carbons (around 285 eV) drastically reduced from 39.72 to 18% and were replaced by CF_2 at 290.47 eV and CF_3 bonding at 292.07 eV at 9.56 and 5.28%, respectively, indicating that oxygen-bonded carbons were replaced by fluorine-bonded carbons. Analysis of the peaks produced elemental contents of carbon and fluorine in the fluorinated carbon (Table 2), which were consistent with the stoichiometry of C_2F .^{65,66,69}

Upon fluorine addition to the surface of carbon, the bonding structure on the side surface of the carbon changes from polyaromatic to polyene like with the π bonds activated by the electron-withdrawing effect of fluorine substituents. The

Table 2. Binding Energy of Various Carbon Species⁶⁹

	20 min	30 min
C–C	42.50	42.37
C–O	39.72	18.00
C–F	13.58	13.25
C(O)F	04.20	10.90
CF_2		09.56
CF_3		05.28

electronic configuration of a large number of sidewall carbons also transforms from the sp^2 into the sp^3 state due to the attached fluorine. The sidewall C–F bond in fluorocarbons is much weaker than in alkyl fluorides and, therefore, can easily dissociate when heat and shear force are applied. The proposed mechanism for plasma-modified carbon interfacing with PP can be explained in schematic Figure 8. This process facilitates a chemical interface where PP is directly attached to the carbon allowing for better load transfer from the surrounding matrix to the stronger filler acting more effectively as the reinforcing member of the composite. The improvement in adhesion contributes to better mechanical and thermal properties. The use of high shear mixing during the processing stage not only disrupts the bundles and disperses the carbon throughout the polymer matrix but also initiates, under high-temperature conditions, an in situ reaction very likely leading to formation of covalent bonds between the carbon and the polymer matrix as proposed in Figure 8.

DSC analysis of biochar carbon-reinforced composites revealed that the typical endothermic melting was at ~ 162 °C and exothermic crystallization was between ~ 114 and 120 °C (Figure 9). With the addition of biochar, there was a slight increase in melting temperature, due to the thermal stability of the filler material. However, in the case of untreated filler composites, melting enthalpy did not increase, which might be due to an improper interface between the polymer and filler.⁶⁷ With plasma-treated composites, the energy required to melt also increased. The highest melting temperature was reported to be 162.05 °C for 1 wt % loaded samples and melting enthalpy was reported to be 106.10 J/g for the 0.5 wt % loaded sample. This is attributed to not only the inclusion and increment of thermally stable biochar but also effective reinforcement through better chemical bonding between the filler carbon and host polymer. The crystallization temper-

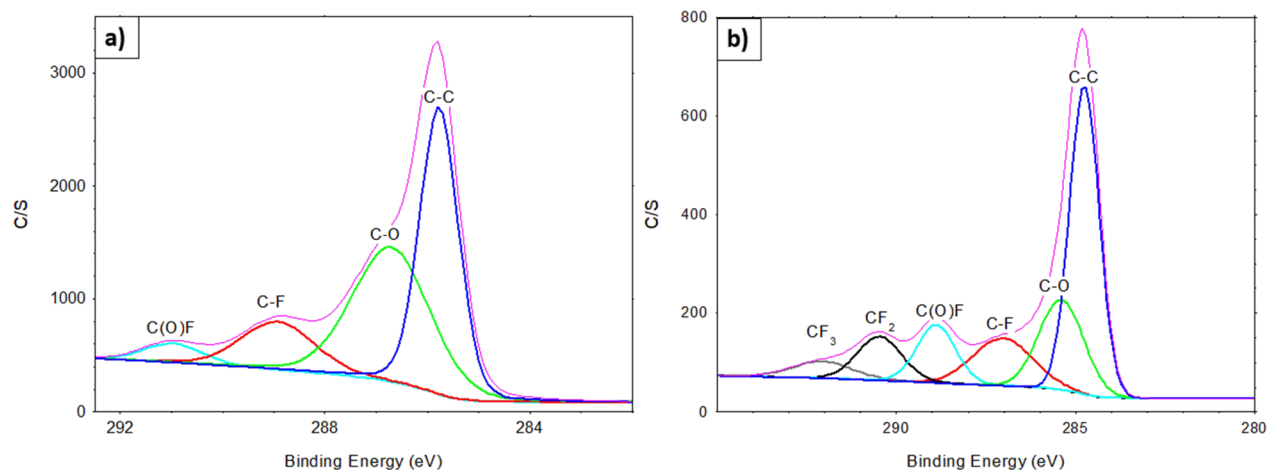


Figure 7. XPS C 1s curve of the fluorine plasma-treated sample after (a) 20 min and (b) 30 min of treatment.

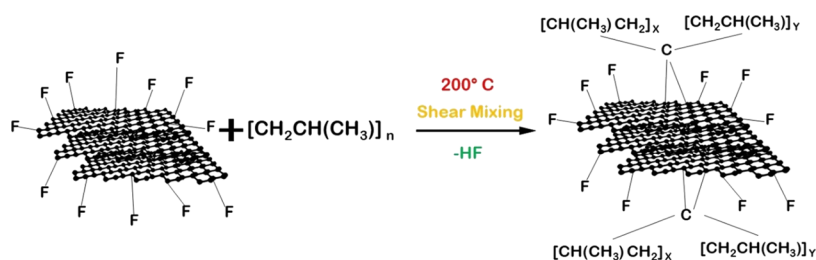


Figure 8. Schematic of proposed covalent bonding of PP to fluorinated biochar during the extrusion process.

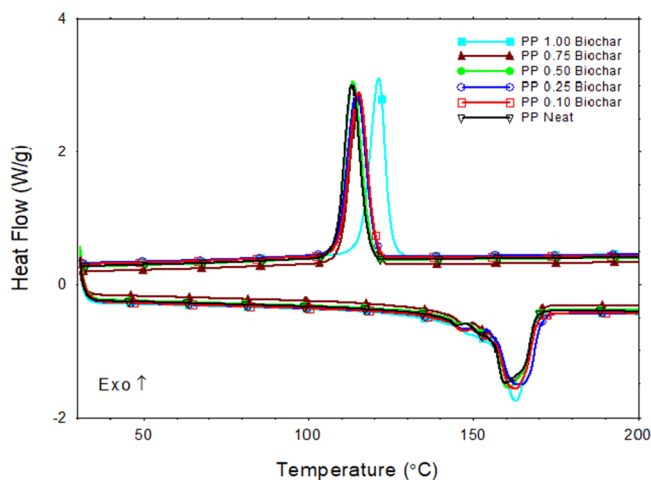


Figure 9. DSC thermographs of the plasma-treated biochar carbon-reinforced PP composite.

atures, on the other hand, were pushed to a higher temperature for all samples compared to that of neat PP. This is most probably due to the nucleation effect of the biochar particles in the PP matrix. The biochar particles acted as points from where crystal growth initiated. In the case of plasma-treated carbon, the energy required for crystallization was slightly higher due to the formation of covalent bonds between the carbon and polymer. A detailed comparison of various thermal properties of the biochar/PP composite is shown in Table 3 below.

TGA analysis (Figure 10) of biochar carbon-reinforced composites revealed that the thermal properties of all the composites improved when compared with neat PP. However, in the case of plasma-treated composites, there was increased thermal stability, which could be due to the effective interface between the carbon filler material and polymer matrix with the

presence of fluorine functionalities. It was observed that the plasma-treated 1 wt % loaded samples demonstrated the best thermal stability when compared with neat samples. The onset of decomposition was delayed by 60 °C, and the maximum rate of decomposition temperature was delayed by 50 °C. Such improved thermal stability in plasma-treated samples is mainly due to the inherent thermal stability of highly crystalline filler carbon and effective reinforcement between the filler and polymer due to the presence of fluorine-activated interactions during the extrusion process. A detailed comparison of thermal properties like the onset of decomposition, max rate of decomposition temperature, and residue are tabulated in Table 4.

The mechanical tests of biochar-reinforced samples revealed that plasma-functionalized biochar was highly effective in reinforcing the material (Figure 11). The brittle failure that was observed in the samples without treatment⁶⁷ was absent. Instead, a more pronounced plastic region was observed suggesting improved reinforcement between the polymer and matrix. In addition to improvement in elongation strength, the modulus of plasma-treated reinforced samples also improved. This is a direct result in improved crystallinity of samples due to covalent interactions between biochar and the polymer matrix. The highest modulus was achieved for 1 wt % loaded samples of 0.65 GPa, which was an increase of 71% when compared with the neat PP polymer. Tensile strength was recorded the highest for the 0.75 wt % loaded sample at a value of 41.49 MPa, which is an improvement of about 90% when compared to neat samples. Especially when comparing the elongation at break, which is a major attribute to confirm improved ductile behavior of the material, it can be observed that for 1 wt % loaded samples, % elongation increased from 12.27 to 38.78, which is an increase of impressive 216%, making this material ideal for engineering applications. The primary mechanism of reinforcement in these samples is through the formation of covalent interactions between the

Table 3. Thermal Properties of the Plasma-Treated Biochar Carbon-Reinforced PP Composite Obtained via DSC

composite sample	T_c (°C)	ΔH_c (J/g)	T_m (°C)	ΔH_m (J/g)	χ_C (%)	
PP Neat	113.22	98.84	159.72	98.10	47.39	63
PP 0.10 USPWC	113.54	105.20	160.04	99.76	48.24	63
PP 0.25 USPWC	114.59	103.50	160.97	99.33	48.11	63
PP 0.50 USPWC	114.83	99.77	161.22	99.07	48.10	63
PP 0.75 USPWC	115.30	96.43	161.65	97.36	47.39	63
PP 1.00 USPWC	115.41	100.10	161.13	101.00	49.29	63
PP 0.10 USFPWC	115.18	102.90	162.50	101.60	49.13	this work
PP 0.25 USFPWC	114.61	103.40	164.03	101.70	49.25	this work
PP 0.50 USFPWC	113.49	103.20	160.43	106.10	51.51	this work
PP 0.75 USFPWC	115.35	103.80	162.05	105.20	51.21	this work
PP 1.00 USFPWC	121.28	103.40	162.90	104.10	50.80	this work

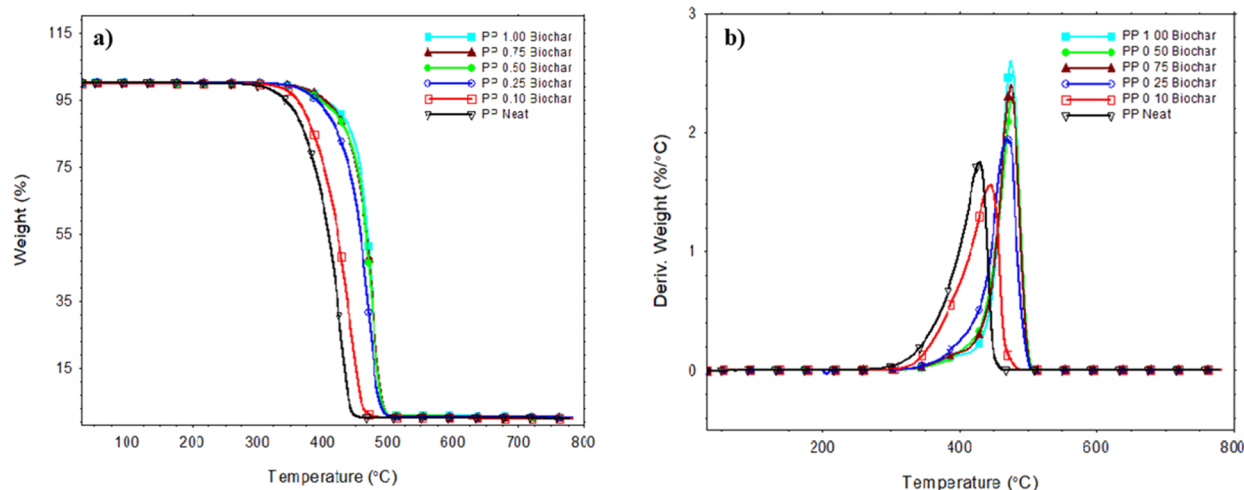


Figure 10. TGA thermographs of the plasma-treated biochar carbon-reinforced PP composite: (a) weight and (b) derivative weight.

Table 4. Thermal Properties of the Plasma-Treated Biochar Carbon-Reinforced PP Composite Obtained via TGA

composite sample	decomp onset temp (°C)	max rate of decomp temp (°C)	% residue @ 750 °C	
PP Neat	342.39	428.59	0.04	63
PP 0.10 USPWC	361.18	443.71	0.09	63
PP 0.25 USPWC	380.16	467.11	0.15	63
PP 0.50 USPWC	385.95	464.35	0.16	63
PP 0.75 USPWC	393.83	469.06	0.19	63
PP 1.00 USPWC	392.19	468.63	0.31	63
PP 0.10 USFPWC	360.34	444.77	0.08	this work
PP 0.25 USFPWC	385.71	472.39	0.10	this work
PP 0.50 USFPWC	395.13	474.81	0.11	this work
PP 0.75 USFPWC	400.92	474.81	0.27	this work
PP 1.00 USFPWC	402.26	477.11	0.33	this work

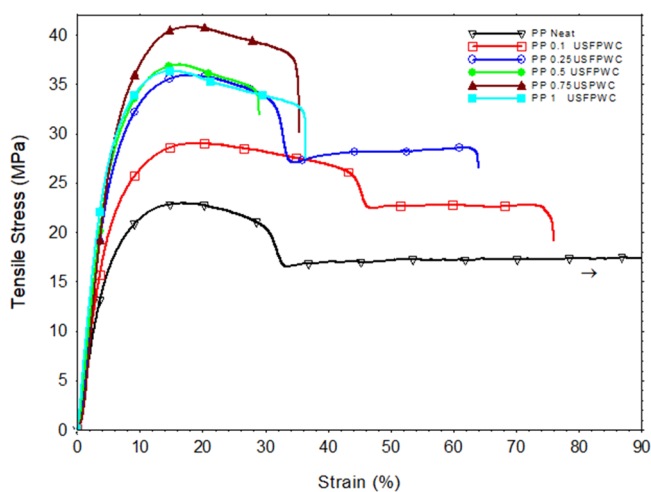


Figure 11. Representative stress–strain curves of the plasma-treated biochar-reinforced PP composite.

biochar and polymer. Detailed comparison of various mechanical properties of PP composites reinforced with biochar with and without plasma treatment is tabulated in Table 5.

Table 5. Mechanical Properties of the Plasma-Treated Biochar Carbon-Reinforced PP Composite

sample	Young's modulus (GPa)	tensile strength (MPa)	elongation at break (%)	
PP Neat	0.38 ± 0.02	21.73 ± 1.22	212.54 ± 17.23	63
PP 0.10 USPWC	0.46 ± 0.04	26.62 ± 2.36	16.35 ± 5.36	63
PP 0.25 USPWC	0.48 ± 0.03	27.21 ± 1.24	16.06 ± 2.32	63
PP 0.50 USPWC	0.50 ± 0.01	28.32 ± 2.36	16.98 ± 1.54	63
PP 0.75 USPWC	0.51 ± 0.01	31.62 ± 0.32	17.01 ± 1.67	63
PP 1.00 USPWC	0.58 ± 0.04	26.59 ± 2.47	12.27 ± 1.98	63
PP 0.10 USFPWC	0.51 ± 0.06	28.55 ± 2.29	77.23 ± 2.45	this work
PP 0.25 USFPWC	0.53 ± 0.07	35.54 ± 1.25	64.36 ± 3.12	this work
PP 0.50 USFPWC	0.56 ± 0.05	36.56 ± 1.98	28.59 ± 7.98	this work
PP 0.75 USFPWC	0.59 ± 0.02	41.49 ± 2.46	37.43 ± 3.59	this work
PP 1.00 USFPWC	0.65 ± 0.04	36.89 ± 3.54	38.78 ± 4.98	this work

Failure analysis of failed samples revealed that plasma functionalization of biochar was effective in reinforcing the polymer matrix. For samples without plasma treatments (Figure 12a), biochar was embedded with the neat surface without any polymer adhering or a clear indication of filler pullout confirming that there was the absence of strong chemical interaction; hence, reinforcement heavily depends on mechanical interlocking. However, in the case of plasma-treated samples, this was evident from the surface of biochar where the polymer was still adhering as shown in Figure 12b, confirming a strong interaction between the polymer and filler. The biochar was still embedded in the polymer, indicating that it acted as resistance to failure (see Figure 12c,d). This was due to effective covalent bond formation at the interface of the

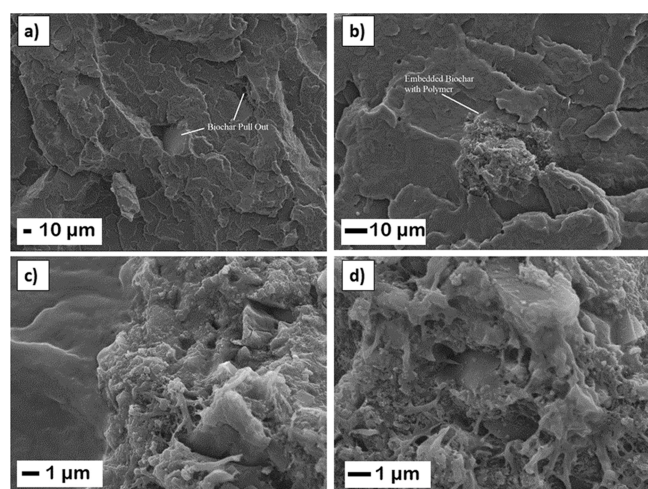


Figure 12. SEM micrograph of the failed biochar-reinforced PP filament: (a) without plasma treatment 0.50%, (b, c) with plasma treatment 0.5 wt %, and (d) with plasma treatment 0.75 wt %.

material. This interaction led to improved thermal and mechanical properties of the overall composite.

Tensile experiments on plasma-treated biochar-reinforced 3D printed dog bone composite samples demonstrated that the biochar filler increased the tensile modulus of all samples (Table 6). The modulus increase was mostly because of the

Table 6. Mechanical Properties of the Biochar Carbon-Reinforced PP 3D Printed Composite

sample	Young's modulus (GPa)	tensile strength (MPa)	elongation at break (%)	
PP Neat	0.041 ± 0.007	5.01 ± 1.59	11.02 ± 2.55	63
PP 0.10 USPWC	0.069 ± 0.003	10.80 ± 4.66	12.68 ± 3.98	63
PP 0.25 USPWC	0.090 ± 0.011	18.70 ± 6.16	13.01 ± 2.73	63
PP 0.50 USPWC	0.111 ± 0.010	16.73 ± 2.56	15.18 ± 3.97	63
PP 0.75 USPWC	0.115 ± 0.004	13.01 ± 6.32	09.49 ± 0.06	63
PP 1.00 USPWC	0.128 ± 0.002	26.03 ± 3.32	22.11 ± 1.43	63
PP 0.10 USFPWC	0.071 ± 0.024	12.69 ± 7.36	13.52 ± 6.21	this work
PP 0.25 USFPWC	0.101 ± 0.019	18.54 ± 8.24	15.96 ± 6.32	this work
PP 0.50 USFPWC	0.117 ± 0.015	20.68 ± 5.95	23.49 ± 8.19	this work
PP 0.75 USFPWC	0.123 ± 0.012	18.37 ± 4.87	12.64 ± 1.77	this work
PP 1.00 USFPWC	0.135 ± 0.016	15.65 ± 9.44	15.11 ± 2.46	this work

inherent material property of the semicrystalline carbon biochar deployed as the filler, as well as the interaction between the filler and the matrix. The modulus value grew in direct proportion to the loading percentages, a trend that was also observed in filament samples. The tensile strength of composite samples was higher than that of neat samples. However, unlike filament samples, there was no noticeable trend in the strength values. The main cause of the poor characteristics of neat PP samples could be dimensional instability following 3D printing, mainly due to shrinkage/

warpage. When compared to untreated filler samples, plasma treatments improved the strength and elongation properties of 3D printed components. However, unlike in the case of filament samples, the improvement was not significant. The underlying issue here is with the printing of PP. As a result, plasma treatments are helpful in reinforcing the matrix with a better filler/matrix interface, but there is still work to be done in optimizing the interface between each printed layer. Researchers have previously discovered a similar issue with PP material printing. As the polymer melt cools after deposition, the volume of the polymer (both free volume between molecular chains and vibrational volume) decreases, resulting in material shrinkage as long as the temperature remains above glass transition.⁵⁹ As a result of the material shrinkage, 3D printed layers lose their capacity to adhere to construct layers. It was proposed that, in order to achieve high interfacial bonding in adjacent layers, the interface between the freshly deposited material and previously deposited material should pass through the crystallization temperature and reach the polymer's melting temperature, allowing for short-term melting of crystalline areas of adjacent layers.⁷⁰ Filler material addition can slow down volumetric change in molecular chains and inhibit quick crystallization of polymer melt. As a result, it was discovered that when the biochar filler material was added, shrinkage decreased proportionally to loading percentages, eventually resulting in improved mechanical qualities. However, unlike filament samples, the modulus and strength parameters of 3D printed objects did not follow any particular trend. This could be because 3D printed samples are more heterogeneous and irregular than extruded filaments or injection molded items, resulting in more inconsistency. Better 3D printed samples with improved qualities can be produced using appropriate process improvement approaches and optimization, reflecting a similar trend observed in filaments.

SEM micrographs of failed 3D printed samples revealed that (Figure 13b) plasma treatment of the biochar filler improved

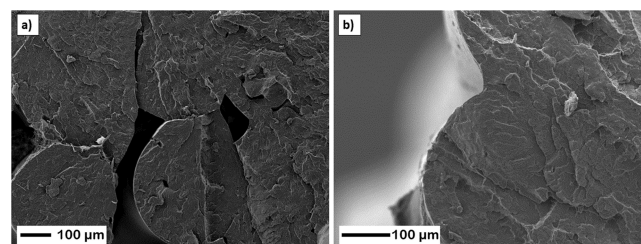


Figure 13. SEM micrograph of the failed 3D printed biochar-reinforced sample (0.50 wt % loading) (a) without plasma treatment and (b) with 30 min plasma treatment.

the interaction between the filler and matrix interface. This helped slightly in achieving a better interface between layers, hence increasing in strength and elongation.

CONCLUSIONS

Biochar made from sustainable starch-based PW could be used as a reinforcing filler material for the PP matrix, according to the findings of this study. Plasma treatments are a good way to modify the surface characteristics of biochar carbon in a long-term sustainable way. Using a low-temperature plasma treatment approach in the presence of sulfur hexafluoride gas, fluorine-related functionalities were successfully integrated on the surface of the carbon. The functional groups that result

are only present at the surface level; therefore, they have no effect on the filler material's bulk properties. The surface fluorine atoms react with the polymer's hydrocarbons to generate covalent bonds during the extrusion process.

Mechanical and thermal properties were much improved as a result of the better interface between the filler and the host polymer. Plasma-treated biochar carbon-reinforced composites with 0.75 wt % loaded samples performed the best, with a strength of 41.49 MPa, a 91% improvement over neat samples, and a 31.22% improvement over untreated samples. Plasma-treated biochar reinforcement increased thermal characteristics as well. Decomposition onset at 402 °C, a delay of around 60 °C, was optimal for 1 wt % loaded samples. The maximum decomposition temperature was around 477 °C, an improvement of roughly 49 °C. Due to the covalent connection between biochar and the polymer matrix, good interface interactions were formed, according to failure analysis. When compared to inert biochar-reinforced 3D printed materials, plasma-modified biochar-reinforced 3D printed samples had improved mechanical properties. Shrinkage/warpage of 3D printed PP samples, on the other hand, is still a work in progress. In conclusion, plasma treatments of filler materials are a long-term sustainable solution for modifying surface properties and have a wide range of applications for increasing the reinforcing ability and consequently the overall properties of composites.

■ ASSOCIATED CONTENT

SI Supporting Information

The Supporting Information is available free of charge at <https://pubs.acs.org/doi/10.1021/acsomega.2c02372>.

Schematic of the Filabot extruder setup and CAD file of the dog bone tensile specimen (Type 1BA) used for 3D printing (PDF)

Objects printed with the printing speed fixed at 50 mm/s (MP4)

■ AUTHOR INFORMATION

Corresponding Author

Vijaya K. Rangari – Department of Materials Science and Engineering, Tuskegee University, Tuskegee, Alabama 36088, United States; orcid.org/0000-0002-3962-1686; Phone: 334-724-4875; Email: vrangari@tuskegee.edu

Authors

Zaheeruddin Mohammed – Department of Materials Science and Engineering, Tuskegee University, Tuskegee, Alabama 36088, United States

Shaik Jeelani – Department of Materials Science and Engineering, Tuskegee University, Tuskegee, Alabama 36088, United States

Complete contact information is available at:

<https://pubs.acs.org/doi/10.1021/acsomega.2c02372>

Author Contributions

Z.M.: conceptualization, methodology, investigation, data curation, formal analysis, writing – original draft, and writing – review and editing. S.J.: supervision. V.R.: supervision, writing review & editing, and funding acquisition.

Notes

The authors declare no competing financial interest.

■ ACKNOWLEDGMENTS

The authors acknowledge the financial support of NSF-AL-EPSCoR #1655280, GRSP-Alabama EPSCoR, NSF-CREST# 1735971, and NSF-MRI Award #1531934.

■ REFERENCES

- (1) Olivetti, E. A.; Cullen, J. M. Toward a sustainable materials system. *Science* **2018**, *360*, 1396–1398.
- (2) Keijer, T.; Bakker, V.; Chris Slootweg, J. Circular chemistry to enable a circular economy. *Nat. Chem.* **2019**, *11*, 190–195.
- (3) Guan, Q. F.; Yang, H. B.; Han, Z. M.; Ling, Z. C.; Yu, S. H. An all-natural bioinspired structural material for plastic replacement. *Nat. Commun.* **2020**, *11*, 5401.
- (4) Li, F.; Zhao, K.; Ng, T. S. A.; Dai, Y.; Wang, C. H. Sustainable production of bio-oil and carbonaceous materials from biowaste copyrolysis. *Chem. Eng. J.* **2022**, *427*, No. 131821.
- (5) Idrees, M.; Ahmed, S.; Mohammed, Z.; Korivi, N. S.; Rangari, V. 3D printed supercapacitor using porous carbon derived from packaging waste. *Addit. Manuf.* **2020**, *36*, No. 101525.
- (6) Fic, K.; Platek, A.; Piwek, J.; Frackowiak, E. Sustainable materials for electrochemical capacitors. *Mater. Today* **2018**, *21*, 437–454.
- (7) Okoro, C.; Mohammed, Z.; Jeelani, S.; Rangari, V. Plasticizing effect of biodegradable dipropylene glycol dibenzoate and epoxidized linseed oil on diglycidyl ether of bisphenol A based epoxy resin. *J. Appl. Polym. Sci.* **2021**, *138*, 50661.
- (8) Hembrick-Holloman, V.; Samuel, T.; Mohammed, Z.; Jeelani, S.; Rangari, V. K. Ecofriendly production of bioactive tissue engineering scaffolds derived from egg-and sea-shells. *J. Mater. Res. Technol.* **2020**, *9*, 13729–13739.
- (9) Das, C.; Tamrakar, S.; Kiziltas, A.; Xie, X. Incorporation of biochar to improve mechanical, thermal and electrical properties of polymer composites. *Polymer* **2021**, *13*, 2663.
- (10) Chang, B. P.; Rodriguez-Urbe, A.; Mohanty, A. K.; Misra, M. A comprehensive review of renewable and sustainable biosourced carbon through pyrolysis in biocomposites uses: Current development and future opportunity. *Renew. Sustain. Energy Rev.* **2021**, *152*, No. 111666.
- (11) Yin, S.; Huang, Y.; Deng, C.; Jiao, Y.; Wu, W.; Seidi, F.; Xiao, H. Hierarchically porous biochar derived from orthometric integration of wooden and bacterial celluloses for high-performance electromagnetic wave absorption. *Compos. Sci. Technol.* **2022**, *218*, No. 109184.
- (12) Jiang, C.; Bo, J.; Xiao, X.; Zhang, S.; Wang, Z.; Yan, G.; Wu, Y.; Wong, C.; He, H. Converting waste lignin into nano-biochar as a renewable substitute of carbon black for reinforcing styrene-butadiene rubber. *Waste Manage.* **2020**, *102*, 732–742.
- (13) Das, O.; Sarmah, A. K.; Bhattacharyya, D. Biocomposites from waste derived biochars: Mechanical, thermal, chemical, and morphological properties. *Waste Manage.* **2016**, *49*, 560–570.
- (14) Gupta, A.; Mohanty, A. K.; Misra, M. Biocarbon from spent coffee ground and their sustainable biocomposites with recycled water bottle and bale wrap: A new life for waste plastics and waste food residues for industrial uses. *Compos. Part A: Appl. Sci. Manuf.* **2022**, *154*, No. 106759.
- (15) Poulouse, A. M.; Elnour, A. Y.; Anis, A.; Shaikh, H.; Al-Zahrani, S. M.; George, J.; Al-Wabel, M. I.; Usman, A. R.; Ok, Y. S.; Tsang, D. C.; Sarmah, A. K. Date palm biochar-polymer composites: An investigation of electrical, mechanical, thermal and rheological characteristics. *Sci. Total Environ.* **2018**, *619-620*, 311–318.
- (16) Zhang, Q.; Khan, M. U.; Lin, X.; Cai, H.; Lei, H. Temperature varied biochar as a reinforcing filler for high-density polyethylene composites. *Compos., Part B: Eng.* **2019**, *175*, No. 107151.
- (17) Das, O.; Kim, N. K.; Kalamkarov, A. L.; Sarmah, A. K.; Bhattacharyya, D. Biochar to the rescue: Balancing the fire performance and mechanical properties of polypropylene composites. *Polym. Degrad. Stab.* **2017**, *144*, 485–496.

- (18) Das, O.; Bhattacharyya, D.; Hui, D.; Lau, K. T. Mechanical and flammability characterisations of biochar/polypropylene biocomposites. *Compos., Part B: Eng.* **2016**, *106*, 120–128.
- (19) Zhang, Q.; Xu, H.; Lu, W.; Zhang, D.; Ren, X.; Yu, W.; Wu, J.; Zhou, L.; Han, X.; Yi, W.; Lei, H. Properties evaluation of biochar/high-density polyethylene composites: Emphasizing the porous structure of biochar by activation. *Sci. Total Environ.* **2020**, *737*, No. 139770.
- (20) Alhelal, A.; Mohammed, Z.; Jeelani, S.; Rangari, V. K. 3D printing of spent coffee ground derived biochar reinforced epoxy composites. *J. Compos. Mater.* **2021**, *55*, 3651–3660.
- (21) Idrees, M.; Jeelani, S.; Rangari, V. Three-dimensional-printed sustainable biochar-recycled PET composites. *ACS Sustainable Chem. Eng.* **2018**, *6*, 13940–13948.
- (22) Sajjadi, B.; Chen, W.-Y.; Egiebor, N. O. A comprehensive review on physical activation of biochar for energy and environmental applications. *Rev. Chem. Eng.* **2019**, *35*, 735–776.
- (23) Sun, Y.; Iris, K. M.; Tsang, D. C.; Fan, J.; Clark, J. H.; Luo, G.; Zhang, S.; Khan, E.; Graham, N. J. Tailored design of graphitic biochar for high-efficiency and chemical-free microwave-assisted removal of refractory organic contaminants. *Chem. Eng. J.* **2020**, *398*, No. 125505.
- (24) Sajjadi, B.; Chen, W. Y.; Mattern, D. L.; Hammer, N.; Dorris, A. Low-temperature acoustic-based activation of biochar for enhanced removal of heavy metals. *J. Water Process Eng.* **2020**, *34*, No. 101166.
- (25) Stankovich, S.; Dikin, D. A.; Piner, R. D.; Kohlhaas, K. A.; Kleinhammes, A.; Jia, Y.; Wu, Y.; Nguyen, S. T.; Ruoff, R. S. Synthesis of graphene-based nanosheets via chemical reduction of exfoliated graphite oxide. *Carbon* **2007**, *45*, 1558–1565.
- (26) Lyu, H.; Gao, B.; He, F.; Zimmerman, A. R.; Ding, C.; Huang, H.; Tang, J. Effects of ball milling on the physicochemical and sorptive properties of biochar: Experimental observations and governing mechanisms. *Environ. Pollut.* **2018**, *233*, 54–63.
- (27) Xiao, J.; Hu, R.; Chen, G. Micro-nano-engineered nitrogenous bone biochar developed with a ball-milling technique for high-efficiency removal of aquatic Cd (II), Cu (II) and Pb (II). *J. Hazard. Mater.* **2020**, *387*, No. 121980.
- (28) Jian, W.; Lau, D. Understanding the effect of functionalization in CNT-epoxy nanocomposite from molecular level. *Compos. Sci. Technol.* **2020**, *191*, No. 108076.
- (29) Mohammed, Z.; Tcherbi-Narteh, A.; Jeelani, S. Effect of graphene nanoplatelets and montmorillonite nanoclay on mechanical and thermal properties of polymer nanocomposites and carbon fiber reinforced composites. *SN Appl. Sci.* **2020**, *2*, 1959.
- (30) Kochetov, R.; Korobko, A. V.; Andritsch, T.; Morshuis, P. H. F.; Picken, S. J.; Smit, J. J. Modelling of the thermal conductivity in polymer nanocomposites and the impact of the interface between filler and matrix. *J. Phys. D: Appl. Phys.* **2011**, *44*, No. 395401.
- (31) Feng, J.; Venna, S. R.; Hopkinson, D. P. Interactions at the interface of polymer matrix-filler particle composites. *Polymer* **2016**, *103*, 189–195.
- (32) Nuhnen, A.; Dietrich, D.; Millan, S.; Janiak, C. Role of filler porosity and filler/polymer interface volume in metal–organic framework/polymer mixed-matrix membranes for gas separation. *ACS Appl. Mater. Interfaces* **2018**, *10*, 33589–33600.
- (33) Fu, S. Y.; Feng, X. Q.; Lauke, B.; Mai, Y. W. Effects of particle size, particle/matrix interface adhesion and particle loading on mechanical properties of particulate–polymer composites. *Compos., Part B: Eng.* **2008**, *39*, 933–961.
- (34) Ma, P. C.; Siddiqui, N. A.; Marom, G.; Kim, J. K. Dispersion and functionalization of carbon nanotubes for polymer-based nanocomposites: A review. *Compos. Part A: Appl. Sci. Manuf.* **2010**, *41*, 1345–1367.
- (35) Cha, J.; Jin, S.; Shim, J. H.; Park, C. S.; Ryu, H. J.; Hong, S. H. Functionalization of carbon nanotubes for fabrication of CNT/epoxy nanocomposites. *Mater. Des.* **2016**, *95*, 1–8.
- (36) Thakur, V. K.; Yan, J.; Lin, M. F.; Zhi, C.; Golberg, D.; Bando, Y.; Sim, R.; Lee, P. S. Novel polymer nanocomposites from bioinspired green aqueous functionalization of BNNTs. *Polym. Chem.* **2012**, *3*, 962–969.
- (37) Raji, M.; Mekhzoum, M. E. M.; Rodrigue, D.; Bouhfid, R. Effect of silane functionalization on properties of polypropylene/clay nanocomposites. *Compos., Part B: Eng.* **2018**, *146*, 106–115.
- (38) Thakur, S.; Karak, N. Ultratough, ductile, castor oil-based, hyperbranched, polyurethane nanocomposite using functionalized reduced graphene oxide. *ACS Sustainable Chem. Eng.* **2014**, *2*, 1195–1202.
- (39) Barbera, V.; Bernardi, A.; Palazzolo, A.; Rosengart, A.; Brambilla, L.; Galimberti, M. Facile and sustainable functionalization of graphene layers with pyrrole compounds. *Pure Appl. Chem.* **2018**, *90*, 253–270.
- (40) Xie, J.; Zhu, C. *Sustainable C (sp³)-H Bond Functionalization*; Springer: Heidelberg, 2016.
- (41) Santoro, S.; Marrocchi, A.; Lanari, D.; Ackermann, L.; Vaccaro, L. Towards Sustainable C–H Functionalization Reactions: The Emerging Role of Bio-Based Reaction Media. *Chem.–Eur. J.* **2018**, *24*, 13383–13390.
- (42) Montanari, C.; Olsén, P.; Berglund, L. A. Interface tailoring by a versatile functionalization platform for nanostructured wood biocomposites. *Green Chem.* **2020**, *22*, 8012–8023.
- (43) Lobo, A. O.; Ramos, S. C.; Antunes, E. F.; Marciano, F. R.; Trava-Airoldi, V. J.; Corat, E. J. Fast functionalization of vertically aligned multiwalled carbon nanotubes using oxygen plasma. *Mater. Lett.* **2012**, *70*, 89–93.
- (44) Cho, B. G.; Hwang, S. H.; Park, M.; Park, J. K.; Park, Y. B.; Chae, H. G. The effects of plasma surface treatment on the mechanical properties of polycarbonate/carbon nanotube/carbon fiber composites. *Compos., Part B: Eng.* **2019**, *160*, 436–445.
- (45) Zschoerper, N. P.; Katzenmaier, V.; Vohrer, U.; Haupt, M.; Oehr, C.; Hirth, T. Analytical investigation of the composition of plasma-induced functional groups on carbon nanotube sheets. *Carbon* **2009**, *47*, 2174–2185.
- (46) Bianco, G. V.; Sacchetti, A.; Ingrassio, C.; Giangregorio, M. M.; Losurdo, M.; Capezzuto, P.; Bruno, G. Engineering graphene properties by modulated plasma treatments. *Carbon* **2018**, *129*, 869–877.
- (47) Sun, D. L.; Hong, R. Y.; Wang, F.; Liu, J. Y.; Kumar, M. R. Synthesis and modification of carbon nanomaterials via AC arc and dielectric barrier discharge plasma. *Chem. Eng. J.* **2016**, *283*, 9–20.
- (48) Mohammed, Z.; Jeelani, S.; Rangari, V. Effect of low-temperature plasma treatment on surface modification of polycaprolactone pellets and thermal properties of extruded filaments. *JOM* **2020**, *72*, 1523–1532.
- (49) Sifuentes-Nieves, I.; Macías, R. Y.; Velázquez, G. N.; Velázquez, G.; Hernandez, Z. G.; Morones, P. G.; Hernández-Hernández, E. Biobased sustainable materials made from starch and plasma/ultrasound modified Agave fibers: Structural and water barrier performance. *Int. J. Biol. Macromol.* **2021**, *193*, 2374–2381.
- (50) Chen, C.; Liang, B.; Lu, D.; Ogino, A.; Wang, X.; Nagatsu, M. Amino group introduction onto multiwall carbon nanotubes by NH₃/Ar plasma treatment. *Carbon* **2010**, *48*, 939–948.
- (51) Felten, A.; Bittencourt, C.; Pireaux, J. J.; Van Lier, G.; Charlier, J. C. Radio-frequency plasma functionalization of carbon nanotubes surface O 2, NH 3, and CF 4 treatments. *J. Appl. Phys.* **2005**, *98*, No. 074308.
- (52) Huang, Y. W.; Yu, Q. F.; Li, M.; Sun, S. N.; Zhao, H.; Jin, S. X.; Fan, J.; Wang, J. G. An overview of low-temperature plasma surface modification of carbon materials for removal of pollutants from liquid and gas phases. *Plasma Processes Polym.* **2021**, *18*, No. 2000171.
- (53) Alam, A.; Wan, C.; McNally, T. Surface amination of carbon nanoparticles for modification of epoxy resins: plasma-treatment vs. wet-chemistry approach. *Eur. Polym. J.* **2017**, *87*, 422–448.
- (54) Mohammed, Z.; Jeelani, S.; Rangari, V. Low temperature plasma treatment of rice husk derived hybrid silica/carbon biochar using different gas sources. *Mater. Lett.* **2021**, *292*, No. 129678.
- (55) Wang, T.; Liu, J.; Zhang, Y.; Zhang, H.; Chen, W. Y.; Norris, P.; Pan, W. P. Use of a non-thermal plasma technique to increase the

number of chlorine active sites on biochar for improved mercury removal. *Chem. Eng. J.* **2018**, *331*, 536–544.

(56) Zhang, Z.; Gao, X. Polypropylene Random Copolymer Based Composite Used for Fused Filament Fabrication: Printability and Properties. *Polymer* **2022**, *14*, 1106.

(57) Bertolino, M.; Battezzore, D.; Arrigo, R.; Frache, A. Designing 3D printable polypropylene: Material and process optimisation through rheology. *Addit. Manuf.* **2021**, *40*, No. 101944.

(58) Biswas, M. C.; Chakraborty, S.; Bhattacharjee, A.; Mohammed, Z. 4D printing of shape memory materials for textiles: Mechanism, mathematical modeling, and challenges. *Adv. Funct. Mater.* **2021**, *31*, No. 2100257.

(59) Spoerk, M.; Holzer, C.; Gonzalez-Gutierrez, J. Material extrusion-based additive manufacturing of polypropylene: A review on how to improve dimensional inaccuracy and warpage. *J. Appl. Polym. Sci.* **2020**, *137*, 48545.

(60) Kalaitzidou, K.; Fukushima, H.; Drzal, L. T. A new compounding method for exfoliated graphite–polypropylene nanocomposites with enhanced flexural properties and lower percolation threshold. *Compos. Sci. Technol.* **2007**, *67*, 2045–2051.

(61) Shubhra, Q. T. H.; Alam, A. K. M. M.; Quaiyyum, M. A. Mechanical properties of polypropylene composites: A review. *J. Thermoplast. Compos. Mater.* **2013**, *26*, 362–391.

(62) Shirvanimoghaddam, K.; Balaji, K. V.; Yadav, R.; Zabihi, O.; Ahmadi, M.; Adetunji, P.; Naebe, M. Balancing the toughness and strength in polypropylene composites. *Compos., Part B: Eng.* **2021**, *223*, No. 109121.

(63) Tressaud, A.; Durand, E.; Labrugère, C.; Kharitonov, A. P.; Kharitonova, L. N. Modification of surface properties of carbon-based and polymeric materials through fluorination routes: From fundamental research to industrial applications. *J. Fluor. Chem.* **2007**, *128*, 378–391.

(64) Tressaud, A.; Durand, E.; Labrugère, C. Surface modification of several carbon-based materials: comparison between CF₄ rf plasma and direct F₂-gas fluorination routes. *J. Fluor. Chem.* **2004**, *125*, 1639–1648.

(65) Shofner, M. L.; Khabashesku, V. N.; Barrera, E. V. Processing and mechanical properties of fluorinated single-wall carbon nanotube–polyethylene composites. *Chem. Mater.* **2006**, *18*, 906–913.

(66) McIntosh, D.; Khabashesku, V. N.; Barrera, E. V. Nanocomposite fiber systems processed from fluorinated single-walled carbon nanotubes and a polypropylene matrix. *Chem. Mater.* **2006**, *18*, 4561–4569.

(67) Mohammed, Z.; Jeelani, S.; Rangari, V. Effective reinforcement of engineered sustainable biochar carbon for 3D printed polypropylene biocomposites. *Compos. Part C: Open Access* **2022**, *7*, No. 100221.

(68) Alghyamah, A. A.; Elnour, A. Y.; Shaikh, H.; Haider, S.; Poulouse, A. M.; Al-Zahrani, S. M.; Almasry, W. A.; Park, S. Y. Biochar/polypropylene composites: A study on the effect of pyrolysis temperature on crystallization kinetics, crystalline structure, and thermal stability. *J. King Saud Univ.-Sci.* **2021**, *33*, No. 101409.

(69) Vandencastele, N.; Reniers, F. Plasma-modified polymer surfaces: Characterization using XPS. *J. Electron Spectrosc. Relat. Phenom.* **2010**, *178-179*, 394–408.

(70) Hertle, S.; Drexler, M.; Drummer, D. Additive manufacturing of poly (propylene) by means of melt extrusion. *Macromol. Mater. Eng.* **2016**, *301*, 1482–1493.